

Three-Oscillator Vibrational Band-Gap Renormalization and Band-Tailing in CsPbI₃ Perovskite Nanocrystals

Albert Liu,¹ L. G. Bonato,² Francesco Sessa,¹ Diogo B. Almeida,^{1,3} Erik Isele,⁴ G. Nagamine,³ L. F. Zagonel,³ A. F. Nogueira,² L. A. Padilha,^{3, a)} and Steven T. Cundiff^{1, b)}

¹⁾Department of Physics, University of Michigan, Ann Arbor, Michigan, USA

²⁾Instituto de Química, Universidade Estadual de Campinas, Campinas, São Paulo, Brazil

³⁾Instituto de Física, Universidade Estadual de Campinas, Campinas, São Paulo, Brazil

⁴⁾Department of Electrical Engineering and Computer Science, University of Michigan, Ann Arbor, Michigan, USA

(Dated: 24 April 2022)

The band-gaps of CsPbI₃ and CsPbBr₃ perovskite nanocrystals are measured by absorption spectroscopy at cryogenic temperatures. Anomalous band-gap shifts are observed in both types of nanocrystals, which are modeled accurately by band-gap renormalization due to lattice vibrational modes. An absorption tail forms at low-temperatures for CsPbI₃ nanocrystals, which we attribute to shallow defect states positioned near the valence band-edge.

I. INTRODUCTION

Colloidal nanocrystals, following decades of extensive study, have begun maturing as a material platform for commercial applications such as displays¹ and photovoltaics². However, despite more than 30 years of research into alternative material platforms, the initial chalcogenide-based colloidal nanocrystals have remained superior in both performance and stability for practical devices. Recently, synthesis of cesium lead-halide perovskite nanocrystals was achieved³, which have generated much excitement due to their exceptional optical properties.

In addition to optical properties translated from bulk perovskites, such as large absorption cross-sections and high quantum efficiencies, perovskite nanocrystals have unique characteristics of their own. Recent examples include superfluorescence from superlattices⁴ and coherent single photon emission from single nanocrystals⁵. Many of these phenomena are studied at cryogenic temperatures, though our understanding of the fundamental physics in this regime is limited.

Here, we study CsPbI₃ and CsPbBr₃ perovskite nanocrystal ensembles at cryogenic temperatures. Absorption spectra reveal an anomalous band-gap shift to higher energies with increasing temperature, which we attribute to band-gap renormalization via electron-phonon coupling. A low-energy absorption tail is also observed in CsPbI₃ that is likely due to shallow trap states, which implies that iodide perovskite nanocrystals may be less defect-tolerant than their bromide counterparts at low temperatures.

II. EXPERIMENT

The orthorhombic perovskite lattice structure of the CsPbI₃ nanocrystals^{6–8} is shown in Fig. 1(a), and transmission electron micrographs of the nanocrystals are shown in Fig. 1(b).

Measurement of 100 nanocrystals informs an average side length of 8.7 ± 2.6 nm. The CsPbBr₃ nanocrystals likewise assume an orthorhombic lattice with an average side length of 8.2 ± 2.4 nm.

The CsPbI₃ nanocrystals are synthesized according to the procedures detailed by Protesescu, et al.^{3,9}. Briefly, 100 mg of PbI₂ (≈ 0.217 mM) are added to a 50 mL 3-neck round-flask, followed by the addition of 4.5 mL of 1-octadecene. The flask is connected to a Schlenk line and vigorously stirred under vacuum at 100°C for 30 min. Afterwards 1 mL of oleic acid and 0.5 mL of oleylamine is added while keeping the reaction flask under vigorous stirring in vacuum at 100°C until complete solubilization of the PbI₂ (indicated by a transparent yellow solution). Prior to injection of the Cs⁺ precursor, the temperature of the Pb²⁺/I⁻ precursor solution is raised to 140°C under vigorous stirring and nitrogen flow, followed by swift injection of 0.8 mL of Cs-oleate stock solution. Formation of a red colloidal suspension of CsPbI₃ nanocrystals is then observed. The suspension is immediately submerged in a cold water bath to cool down to room temperature for quenching nanocrystal growth. The nanocrystals are cleaned by adding 15 mL of anhydrous methylacetate and centrifuged at 12000 rpm for 5 minutes. The supernatant is discarded and the precipitated nanocrystals are dispersed in anhydrous hexane. An absorption peak is then observed at the band-edge, which reflects a narrow nanocrystal size distribution.

CsPbBr₃ nanocrystals were also synthesized according to the method of Protesescu et al., but a distinct 1S exciton absorption peak was not observed due to a broad size distribution (see Supplementary Material). We therefore study bromide nanocrystals synthesized via the method detailed in Yassitepe et al.¹⁰ which offers superior size dispersion control and results in an absorption peak. Comparable band-gap temperature shifts of nanocrystals synthesized via both methods indicate similar underlying electron-phonon dynamics.

To study their optical properties at cryogenic temperatures we redisperse the nanocrystals in heptamethylnonane, a branched alkane that forms a transparent glass at cryogenic temperatures¹². The colloidal suspension is held in a custom sample holder approximately 0.5 mm in thickness and mounted to a cold-finger cryostat. Absorption spectra are then

^{a)}Electronic mail: padilha@ifi.unicamp.br

^{b)}Electronic mail: cundiff@umich.edu

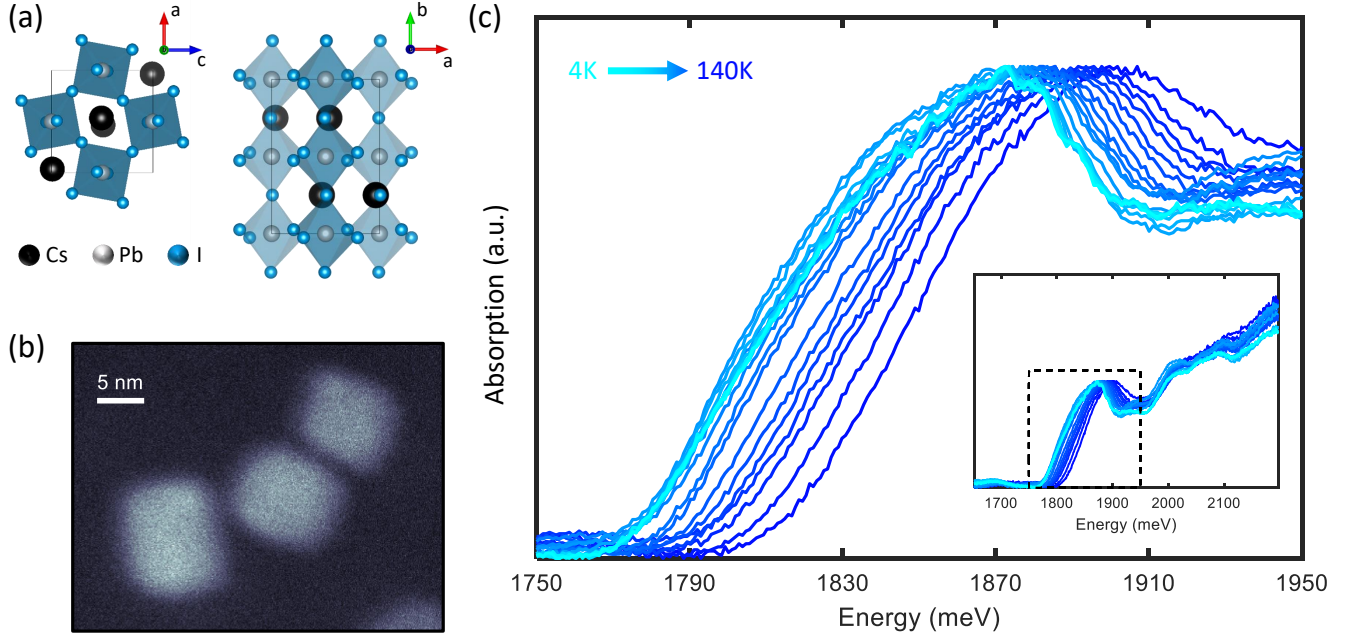


FIG. 1. (a) Two perspective views of the orthorhombic perovskite lattice structure of CsPbI₃ with axes as shown (plotted using the VESTA software¹¹). The unit cell is denoted by the solid black lines. (b) Transmission electron micrograph of nanocrystals. (c) Absorption spectra of CsPbI₃ nanocrystals at temperatures ranging from 4 K to 140 K as indicated. The full-range spectra are plotted inset, while the 1S exciton peak outlined by the dashed box is shown in the main plot. The specific temperatures plotted are indicated by the data in Fig. 2(b).

measured with a broadband white light source and a UV-vis diode array spectrometer.

III. RESULTS AND DISCUSSION

CsPbI₃ absorption spectra normalized to the lowest-energy 1S exciton absorption peak at temperatures ranging from 4 K to 140 K are plotted in Fig. 1(c). Although multiple peaks are observed that correspond to distinct exciton transitions, here we focus on the 1S exciton absorption peak that reflects the fundamental electronic band-gap (energy-gap) of the nanocrystals. As temperature increases the band-gap exhibits a pronounced blue-shift to higher energies, which is contrary to the red-shift observed in most solids. In the literature, this phenomenon has been referred to as an anomalous band-gap shift^{13–16}.

To quantify the band-gap shift, we fit the peaks with Gaussian lineshapes that reflect the size distribution of the nanocrystals. As shown in Fig. 2(a), we fit only the top of each peak due to absorption tails present at lower temperatures. The widths σ , of each Gaussian fit, allowed to vary freely, do not change significantly with temperature (mean width 41.81 meV and standard deviation 3.37 meV). The fitted Gaussian center energies (which agree closely with center energies found from a fourth-order polynomial fit) are plotted in Fig. 2(b), which reveals an interesting behavior at temperatures below 50 K. Specifically, two clear inflection points at 20 and 30 K are observed that reveal more complicated band-gap behavior than previously reported for photoluminescence

measurements of similar perovskite nanocrystals¹⁶.

The dependence of the electronic band-gap on temperature T may be expressed as^{15,17}:

$$E_g(T) = E_0 + AT + \sum_n B_n \left(\frac{1}{e^{\hbar\omega_n/k_B T} - 1} + \frac{1}{2} \right). \quad (1)$$

The first term E_0 is the intrinsic material band-gap at $T = 0$, and the coefficient A in the second term characterizes the change in band-gap due to lattice unit cell expansion/contraction (in the so-called quasi-harmonic approximation¹⁷). Here the change in quantum confinement energy due to expansion/contraction of nanocrystal volume, which we expect to be negligible at low temperatures¹⁸, is ignored. The third term then represents renormalization of the band-gap due to electron-phonon interactions, where n is summed over all phonon branches and all wave-vectors within the Brillouin zone for each branch. B_n and $\hbar\omega_n$ are the electron-phonon coupling strength and vibrational energy respectively for mode n . Whether B_n is positive or negative, resulting in an increase or decrease of the band-gap respectively, arises from a complex interplay of microscopic dynamics and cannot be predicted easily from the properties of a given phonon branch^{13,19}. However, accounting for all possible phonon branches throughout the Brillouin zone is often unnecessary in modeling the behavior of real systems. Instead, one²⁰ or two¹³ vibrational modes are usually assumed dominant (referred to as one-oscillator and two-oscillator models) which reduces the summation to either one or two terms respectively.

Here, we find both the one-oscillator and two-oscillator

models to be insufficient in modeling the band-gap temperature dependence observed for CsPbI₃. As mentioned above, two inflection points are observed that necessitate at least three dominant vibrational modes that independently renormalize the band-gap. A least-squares fit of the band-gap temperature dependence to this three-oscillator model is plotted in Fig. 2(b), where good agreement is observed at both high and low temperatures. The fitted parameters are $E_0 = 1916.9$ meV, $A = 0.3$ meV/K, $\hbar\omega_1 = 5.38$ meV, $\hbar\omega_2 = 5.91$ meV, $\hbar\omega_3 = 17.02$ meV, $B_1 = -698.01$ meV, $B_2 = 821.67$ meV, and $B_3 = -217.39$ meV. Instead of the acoustic and optical phonon categories that are usually invoked for two-oscillator models^{15,16}, a three-oscillator model in perovskite materials align more naturally to the bending, stretching, and rocking perovskite vibrational modes that possess distinct ranges of vibrational energies²¹.

We note that although the two-oscillator model was recently invoked by Saran et al. to model the temperature dependence of photoluminescence center energy in perovskite nanocrystals¹⁶, the data points taken at low temperatures (below 50 K) were too sparse to resolve the two inflection points we observe. Their resultant fitted band-gap dependence is plotted in Fig. 2b for comparison. It is therefore unclear whether the apparent two-oscillator behavior of their measurements on CsPbI₃ was due to coarse-graining or confounding effects of the photoluminescence Stokes shift²².

Lower-energy absorption tails are observed. For ideal nanocrystals, the exciton density of states are comprised of delta functions that result in roughly Gaussian absorption peaks (reflecting the nanocrystal size distribution). Absorption tails at lower-energy are therefore indicative of corresponding tails of the electronic density of states, often attributed to impurities²³ or surface states²⁴. As shown in Fig. 2(a), the absorption peak is Gaussian at 140 K and develops a lower-energy tail with decreasing temperature. We attribute this tail to shallow defect states surrounding the valence band-edge that have been shown to arise from lattice point defects²⁵. At high temperatures valence band electrons populate the band-edge in a thermal equilibrium distribution. At low temperatures those electrons then fill the defect states from lowest energy upwards, which comprise a Halperin-Lax type distribution²⁶ with a $\exp(\sqrt{E})$ dependence^{27,28}. The disappearance of the tail at 140 K thus suggests a few-meV (comparable to the 140 K Boltzmann energy of 12 meV) defect state energy distribution.

The same absorption measurements are then repeated on two CsPbBr₃ samples synthesized via different procedures as described above. The bromide sample synthesized via the method of Protesescu et al. only exhibits a steep band-edge (see Supplementary Material) that does not allow for accurate fitting of the band-gap, but the sample synthesized according to Yassitepe et al.¹⁰ exhibits a distinct absorption peak (as in CsPbI₃). As shown in Fig. 3a, no band-tailing is observed to form at any temperature. We note that the increased noise of these spectra, compared to the CsPbI₃ spectra shown in Fig. 2a, is due to the position of the CsPbBr₃ nanocrystal band-gap near the edge of our white light spectrum.

The fitted band-gap energies are plotted in Fig. 3b, which

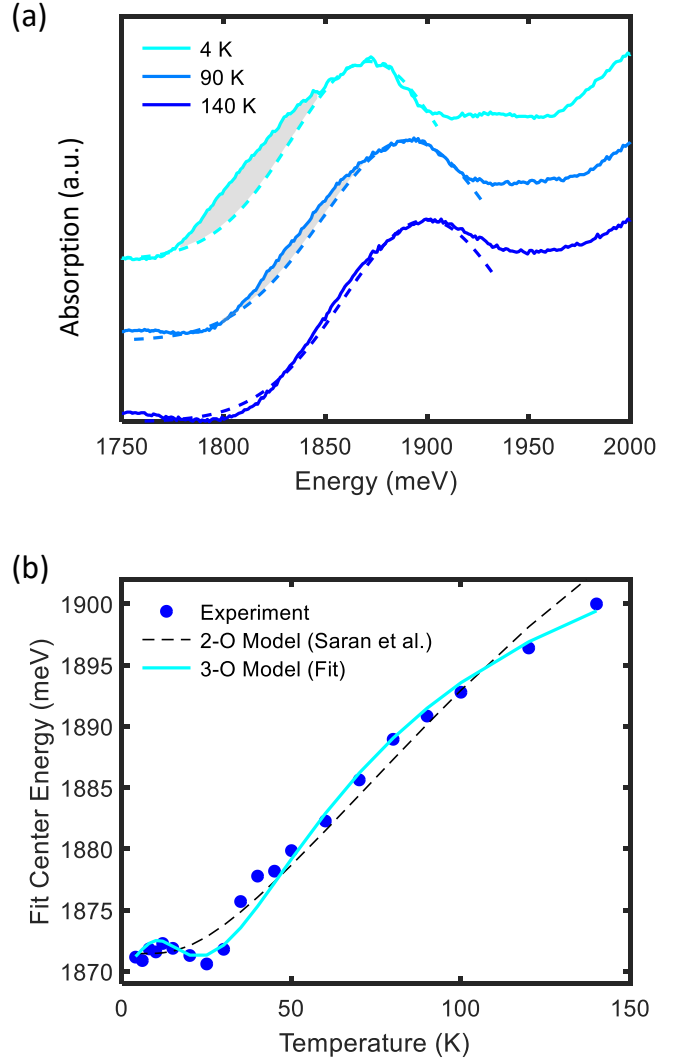


FIG. 2. (a) Gaussian peak fits of CsPbI₃ absorption spectra at three representative temperatures 4, 90, and 140 K. A low-energy absorption tail, indicated by the shaded gray region, forms at low temperature. (b) Dark-blue dots show fitted Gaussian center energy as a function of temperature, which reflects the material band-gap. A two-oscillator (2-O) model using the fitted parameters from Saran et al.¹⁶ and a fit to the three-oscillator (3-O) model described in the text are then plotted as the dashed black curve and solid light-blue curve respectively.

display markedly different behavior at low temperatures. A single subtle inflection point is observed near 50 K, and the trend fits well to a two-oscillator model. The fitted parameters are $E_0 = 2405$ meV, $A = 0.1881$ meV/K, $\hbar\omega_1 = 11.93$ meV, $\hbar\omega_2 = 10.73$ meV, $B_1 = -497.97$ meV, and $B_2 = 451.49$ meV. We note that while our overall band-gap shift is over twice that measured by Saran et al.¹⁶, our shift agrees well with absorption measurements of the other bromide sample synthesized via the method of Protesescu et al.³ (see Supplementary Material). Therefore, the discrepancy may be due to a temperature-dependent Stokes-shift that increases at lower temperatures.

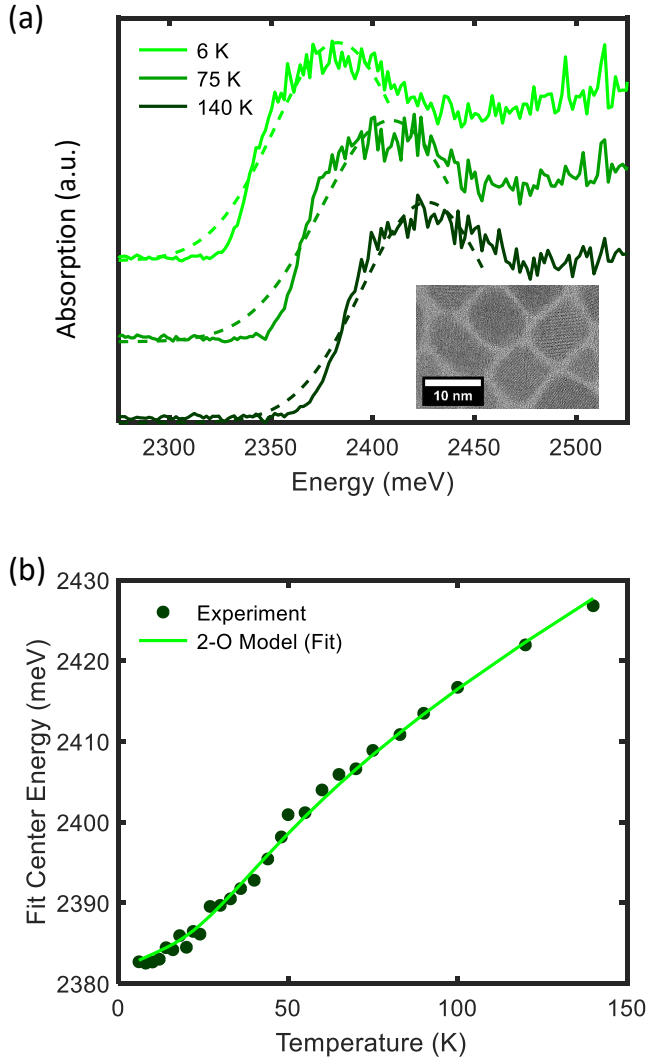


FIG. 3. (a) Gaussian peak fits of CsPbBr₃ absorption spectra at three representative temperatures 6, 75, and 140 K. The absorption peak lineshape does not change significantly with temperature. Inset shows a transmission electron micrograph of the nanocrystals synthesized by the method of Yassitepe et al.¹⁰ (b) Dark-green dots show fitted Gaussian center energy as a function of temperature, which reflects the material band-gap. A fit to the two-oscillator (2-O) model described in the text is then plotted as the solid green curve.

IV. CONCLUSION

In summary, the absorption of CsPbI₃ and CsPbBr₃ perovskite nanocrystals are measured at cryogenic temperatures. In addition to the anomalous band-gap shifts to higher energies with increasing temperature, additional inflection points are observed at low temperatures that we attribute to band-gap renormalization by two vibrational modes in CsPbBr₃ and, contrary to a recent study¹⁶, three vibrational modes in CsPbI₃. Lastly, absorption tails are found to form in CsPbI₃ nanocrystals at low temperatures, which we attribute to defect states surrounding the valence band-edge. While perovskite

nanocrystals have been found to be exceptionally defect-tolerant²⁹, our finding suggests that shallow defects may begin to influence the optical properties of iodide nanocrystals at cryogenic temperatures.

ACKNOWLEDGMENTS

This work was supported by the Department of Energy grant number DE-SC0015782 and by the Sao Paulo Research Foundation, under the grant number 2013/16911-2. D.B.A. and G.N. acknowledge support by fellowships from the Brazilian National Council for Scientific and Technological Development (CNPq). Research was also supported by LNNano/CNPq/MCTIC, where the TEM measurements were performed.

- ¹M. K. Choi, J. Yang, T. Hyeon, and D.-H. Kim, "Flexible quantum dot light-emitting diodes for next-generation displays," *npj Flexible Electronics* **2**, 10 (2018).
- ²M. Yuan, M. Liu, and E. H. Sargent, "Colloidal quantum dot solids for solution-processed solar cells," *Nature Energy* **1**, 16016 EP – (2016), review Article.
- ³L. Protesescu, S. Yakunin, M. I. Bodnarchuk, F. Krieg, R. Caputo, C. H. Hendon, R. X. Yang, A. Walsh, and M. V. Kovalenko, "Nanocrystals of cesium lead halide perovskites (CsPbX₃, X = Cl, Br, and I): Novel optoelectronic materials showing bright emission with wide color gamut," *Nano Letters* **15**, 3692–3696 (2015).
- ⁴G. Rainò, M. A. Becker, M. I. Bodnarchuk, R. F. Mahrt, M. V. Kovalenko, and T. Stöferle, "Superfluorescence from lead halide perovskite quantum dot superlattices," *Nature* **563**, 671–675 (2018).
- ⁵H. Utzat, W. Sun, A. E. K. Kaplan, F. Krieg, M. Ginterseder, B. Spokoyny, N. D. Klein, K. E. Shulenberger, C. F. Perkinson, M. V. Kovalenko, and M. G. Bawendi, "Coherent single-photon emission from colloidal lead halide perovskite quantum dots," *Science* **363**, 1068 (2019).
- ⁶P. Cottingham and R. L. Brutchey, "On the crystal structure of colloidally prepared CsPbBr₃ quantum dots," *Chemical Communications* **52**, 5246–5249 (2016).
- ⁷F. Bertolotti, L. Protesescu, M. V. Kovalenko, S. Yakunin, A. Cervellino, S. J. L. Billinge, M. W. Terban, J. S. Pedersen, N. Masciocchi, and A. Guagliardi, "Coherent nanotwins and dynamic disorder in cesium lead halide perovskite nanocrystals," *ACS Nano* **11**, 3819–3831 (2017).
- ⁸R. J. Sutton, M. R. Filip, A. A. Haghighirad, N. Sakai, B. Wenger, F. Giustino, and H. J. Snaith, "Cubic or orthorhombic?: Revealing the crystal structure of metastable black-phase CsPbI₃ by theory and experiment," *ACS Energy Letters* **3**, 1787–1794 (2018).
- ⁹L. Protesescu, S. Yakunin, S. Kumar, J. Bär, F. Bertolotti, N. Masciocchi, A. Guagliardi, M. Grotevent, I. Shorubalko, M. I. Bodnarchuk, C.-J. Shih, and M. V. Kovalenko, "Dismantling the 'red wall' of colloidal perovskites: Highly luminescent formamidinium and formamidinium-cesium lead iodide nanocrystals," *ACS Nano* **11**, 3119–3134 (2017).
- ¹⁰E. Yassitepe, Z. Yang, O. Voznyy, Y. Kim, G. Walters, J. A. Castañeda, P. Kanjanaboos, M. Yuan, X. Gong, F. Fan, J. Pan, S. Hoogland, R. Comin, O. M. Bakr, L. A. Padilha, A. F. Nogueira, and E. H. Sargent, "Amine-free synthesis of cesium lead halide perovskite quantum dots for efficient light-emitting diodes," *Advanced Functional Materials* **26**, 8757–8763 (2016).
- ¹¹K. Momma and F. Izumi, "VESTA3 for three-dimensional visualization of crystal, volumetric and morphology data," *Journal of Applied Crystallography* **44**, 1272–1276 (2011).
- ¹²A. Liu, D. B. Almeida, W. K. Bae, L. A. Padilha, and S. T. Cundiff, "Non-markovian exciton-phonon interactions in core-shell colloidal quantum dots at femtosecond timescales," *Physical Review Letters* **123**, 057403 (2019).
- ¹³A. Göbel, T. Ruf, M. Cardona, C. T. Lin, J. Wrzesinski, M. Steube, K. Reimann, J.-C. Merle, and M. Joucla, "Effects of the isotopic composition on the fundamental gap of CuCl," *Physical Review B* **57**, 15183–15190 (1998).

- ¹⁴I.-H. Choi and P. Y. Yu, "Suppression of the anomalous blue shift in the band gap temperature dependence of AgCuGaS_2 alloys," *Physical Review B* **63**, 235210 (2001).
- ¹⁵C. Yu, Z. Chen, J. J. Wang, W. Pfenninger, N. Vockic, J. T. Kenney, and K. Shum, "Temperature dependence of the band gap of perovskite semiconductor compound CsSnI_3 ," *Journal of Applied Physics* **110**, 063526 (2011).
- ¹⁶R. Saran, A. Heuer-Jungemann, A. G. Kanaras, and R. J. Curry, "Giant bandgap renormalization and exciton-phonon scattering in perovskite nanocrystals," *Advanced Optical Materials* **5**, 1700231 (2017).
- ¹⁷M. Cardona, "Electron-phonon interaction in tetrahedral semiconductors," *Solid State Communications* **133**, 3–18 (2005).
- ¹⁸N. Moses Badlyan, A. Biermann, T. Aubert, Z. Hens, and J. Maultzsch, "Thermal expansion of colloidal CdSe/CdS core/shell quantum dots," *Physical Review B* **99**, 195425 (2019).
- ¹⁹N. Garro, A. Cantarero, M. Cardona, A. Göbel, T. Ruf, and K. Eberl, "Dependence of the lattice parameters and the energy gap of zinc-blende-type semiconductors on isotopic masses," *Physical Review B* **54**, 4732–4740 (1996).
- ²⁰I.-H. Choi, S.-H. Eom, and P. Y. Yu, "Soft phonon mode and the anomalous temperature dependence of band gap in AgGaS_2 ," *physica status solidi (b)* **215**, 99–104 (1999).
- ²¹M. A. Pérez-Osorio, R. L. Milot, M. R. Filip, J. B. Patel, L. M. Herz, M. B. Johnston, and F. Giustino, "Vibrational properties of the organic-inorganic halide perovskite $\text{CH}_3\text{NH}_3\text{PbI}_3$ from theory and experiment: Factor group analysis, first-principles calculations, and low-temperature infrared spectra," *The Journal of Physical Chemistry C* **119**, 25703–25718 (2015).
- ²²H. Qiao, K. A. Abel, F. C. J. M. van Veggel, and J. F. Young, "Exciton thermalization and state broadening contributions to the photoluminescence of colloidal PbSe quantum dot films from 295 to 4.5 K," *Physical Review B* **82**, 165435 (2010).
- ²³I. Studenyak, M. Kranjec, and M. Kurik, "Urbach rule in solid state physics," *International Journal of Optics and Applications* **4**, 76–83 (2014).
- ²⁴P. Guyot-Sionnest, E. Lhuillier, and H. Liu, "A mirage study of CdSe colloidal quantum dot films, Urbach tail, and surface states," *The Journal of Chemical Physics* **137**, 154704 (2012).
- ²⁵J. Kang and L.-W. Wang, "High defect tolerance in lead halide perovskite CsPbBr_3 ," *The Journal of Physical Chemistry Letters* **8**, 489–493 (2017).
- ²⁶B. I. Halperin and M. Lax, "Impurity-band tails in the high-density limit. I. minimum counting methods," *Physical Review* **148**, 722–740 (1966).
- ²⁷R. Yan, W. Zhang, W. Wu, X. Dong, Q. Wang, and J. Fan, "Optical spectroscopy reveals transition of $\text{CuInS}_2/\text{ZnS}$ to $\text{Cu}_x\text{Zn}_{1-x}\text{InS}_2/\text{ZnS}:\text{Cu}$ alloyed quantum dots with resultant double-defect luminescence," *APL Materials* **4**, 126101 (2016).
- ²⁸J. Jean, T. S. Mahony, D. Bozyigit, M. Sponseller, J. Holovsky, M. G. Bawendi, and V. Bulovic, "Radiative efficiency limit with band tailing exceeds 30% for quantum dot solar cells," *ACS Energy Letters* **2**, 2616–2624 (2017).
- ²⁹H. Huang, M. I. Bodnarchuk, S. V. Kershaw, M. V. Kovalenko, and A. L. Rogach, "Lead halide perovskite nanocrystals in the research spotlight: Stability and defect tolerance," *ACS Energy Letters* **2**, 2071–2083 (2017).